COMSOL Multiphysics® Software as a Metasurfaces Design Tool for Plasmonic-Based Flat Lenses

Bryan M. Adomanis*[1], D. Bruce Burckel[2], and Michael A. Marciniak[1]
[1]Department of Engineering Physics, Air Force Institute of Technology, 2950 Hobson Way, Wright-Patterson Air Force Base, OH 45433-7765
[2]Sandia National Laboratories, P.O. Box 5800, Albuquerque, New Mexico 87185
*Corresponding author: bryan.adomanis@us.af.mil

Abstract: COMSOL Multiphysics® was used to simulate the response of parametrized gold V-antennas on a silicon substrate, which served as a basis for the design of several plasmonics-based metasurface lenses. The simulated phase and amplitude of the scattered, cross-polarized far-field of the scatterer was parametrized over the dipole length $(h/2)$ and vertex angle (Δ) to determine the optimal geometries needed to access the full 2π phase space. These elements were then arrayed linearly according to Fresnel lens phase calculations and formed the basis of a cylindrical focusing optic. Nineteen lenses and eight metasurfaces were fabricated with varying wavelengths, focal lengths, diameters, number of unique elements and packing densities. By validating the lens design using a non-optimized scatterer made of a simple geometry, this effort provided confidence in the future use of COMSOL for a comprehensive investigation of lens design optimization using more complex structures and architectures.

Keywords: metasurfaces, flat lens, plasmonics

1. Introduction

Flat lenses require precise control of a phase gradient across an interface, which is enabled through the application of engineered surfaces, such as metasurfaces [1]. Periodic arrays of plasmonic antennas have been utilized to generate this desired phase gradient [2-8], which dictates the angle of "anomalous" refraction of the cross-polarized field scattered from a normal-incidence beam.

However, the designs utilized to-date have been simple geometries and architectures due to the challenges of numerically modeling more complex forms, and as a result, scattering efficiencies have been unacceptable for real-world application in the infrared (IR) [4, 7, 9, 10]. Therefore, an optimization effort is necessary to improve the lens performance.

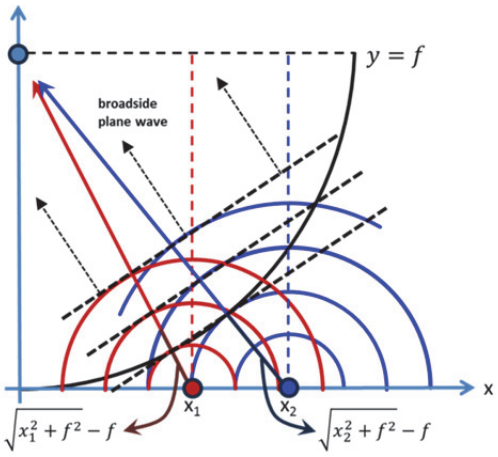

Figure 1. Two point scatterers, with a relative phase difference generating a broadside plane wave.

COMSOL Multiphysics® (COMSOL) has been proposed to accomplish the numerical modeling for these designs, which will serve as a good comparison to previous work done in finite-difference time domain (FDTD) [2-4, 7, 11, 12] and other finite element method (FEM) [9] softwares. In order to establish confidence before proceeding with complex designs, COMSOL was used to generate several simple plasmonics-based flat lens designs, which were then fabricated and measured for validation of the simulated results. These lenses were assessed for characterization of their depth-of-field in the mid- and long-wave infrared (M/LWIR) regime under several changing parameters, such as a changing focal ratio $(\mathcal{F}/\#)$, packing density and number of unique discrete elements used to comprise the resulting phase front.

2. Flat Lens Theory

2.1 Generalized Snell's Law

Refractive optics of a plane wave at the homogeneous interface of two differing bulk media is well understood: in short, phase-

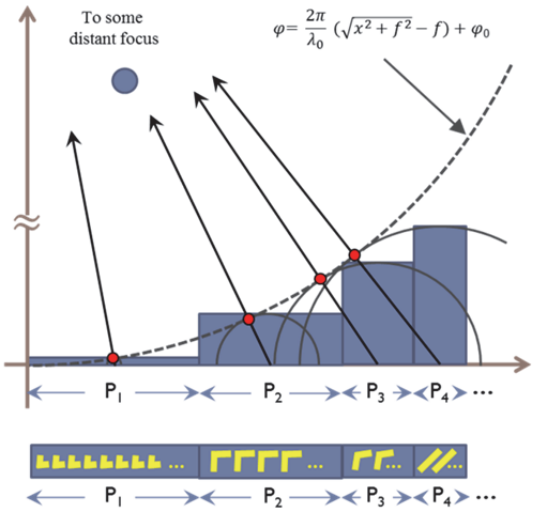

Figure 2. Expanding the scatterer concept of Figure 1 to discrete regions P_i of constant phase for lensing.

matching conditions at the interface demand that an electromagnetic wave bend according to Snell's law, where $n_1 \sin\theta_1 - n_2 \sin\theta_2 = 0$. However, for inhomogeneous interfaces, the phase delay (ϕ) imposed upon a plane wave is no longer translationally invariant across the surface, and thus Snell's law has a more generalized solution, now consisting of a term describing the gradient of the phase discontinuity along the surface [2]. In 1-D this is:

$$n_1 \sin\theta_1 - n_2 \sin\theta_2 = \frac{\lambda}{2\pi}\frac{d}{dx}\Phi[x], \qquad [1]$$

which for a linear gradient ($d^2\Phi/dx^2 = 0$) has been proposed simply as a reimagining of diffraction from a blazed grating [13].

The result is that a normally-incident plane wave ($\theta_1 = 0°$) will couple to a propagating plane wave at some oblique angle ($\theta_2 \neq 0°$) into one of the diffraction modes supported via the linear phase discontinuity. Thus, changing the slope of the gradient will change the broadside angle of propagation, and so an assortment of optical functions can be realized.

A demonstration of this is shown in Figure 1. Two point scatterers, with a relative phase difference generating a broadside plane wave.Figure 1, where two point dipoles radiating at different phases (but equal amplitudes) generate a broadside planar wavefront. As well known in antenna array theory, changing either the separation or the relative scattered phase will change the broadside angle. Expanding this theory to a greater scale and customizability introduces the possibility for lensing, but also requires a look into the structures needed to create such a function.

2.2 Metasurface Lenses

Metasurfaces are arrays of periodic subwavelength structures which can be engineered for a specific electromagnetic response, such as a particular resonance wavelength, bandwidth or scattering phase and amplitude. These factors become the impetus for designing a real-world flat lens, as an individual scattering element can be tailored to give a specific phase delay, and thus, correspondingly, an array of elements can be tailored to give a determinable phase gradient along an interface.

With this in mind, there are two means to array the metasurface elements to generate a lensing function. Looking back to Figure 1, the black semicircle represents the curve spanned by a circle with focal length f as the radius and centered at $(0, f)$. The phase matching condition for neighboring elements to converge constructively at $(0, f)$ is:

$$\Delta\varphi = \varphi_{i+1} - \varphi_i = \frac{2\pi}{N}, \qquad [2]$$

where φ_i is the Fresnel lens phase formula

$$\varphi_i = \frac{2\pi}{\lambda_0}\left(\sqrt{x_i^2 + y_i^2 + f^2} - f\right) + \varphi_0, \quad [3]$$

N is the number of scatterers, i is the scatterer index of the range $\{1, N-1\}$, λ_0 is the freespace wavelength and φ_0 is the phase of the zeroth (central) scatterer. For equally spaced elements of a constant phase gradient—i.e. the metasurface which only bends a plane wave—this condition cannot be met, and so either the phase shift or the element spacing must be non-linear.

The first published metasurface lens implemented the latter approach, in a manner shown in Figure 2, where discrete regions of constant phase P_i spaced non-uniformly were used to meet the phase matching conditions [4]. V-antennas (bottom) were used to provide a known constant phase in the regions and to generate a strong enough scattered response.

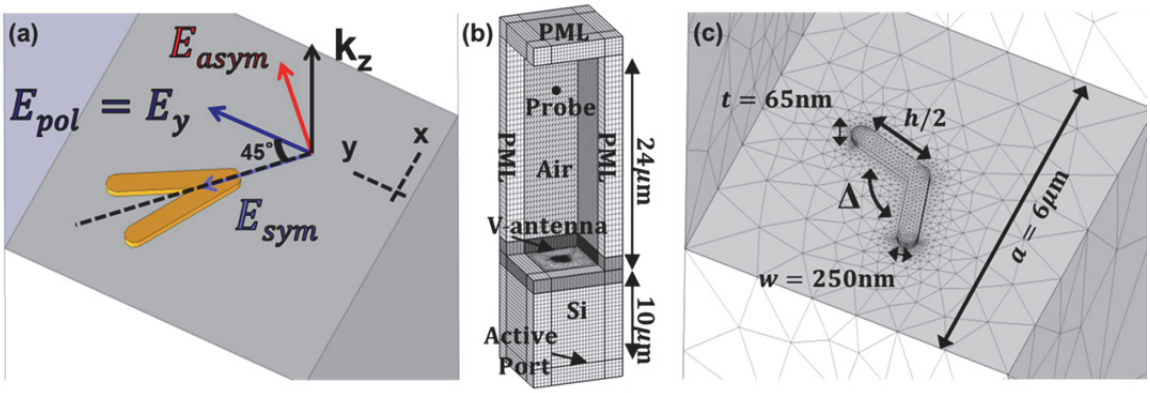

Figure 3. The field components (a), unit cell model (b) and geometries of interest (c) for the 3-D COMSOL V-antenna simulations used to obtain the scattered cross-polarized field over a large parameter space.

3. Use of COMSOL Multiphysics® Software

The focus of this work was to reproduce variants of the first metasurface lens design, using COMSOL to generate a large trade space from which to choose elements that are, unlike previous work, optimized in amplitude [2, 4]. While analytical solutions of the scattered field for a simple V-antenna geometry are available, the intent of this effort was to validate a simple geometry before progressing to more complex geometries.

The goal of the simulations was to obtain the scattered cross-polarized field $\left(\boldsymbol{E}_{scat}^{x-pol}\right)$ of the V-antennas as a function of the vertex angle (Δ) and dipole length (h). From this, the phase $\left(\varphi = Arg[\boldsymbol{E}_{scat}^{x-pol}]\right)$ and amplitude $\left(\left|\boldsymbol{E}_{scat}^{x-pol}\right|\right)$ were extracted to map the scatterer response from a full range of parametrized V-antenna geometries.

The field components, full COMSOL model and scatterer geometries of interest are shown in Figure 3(a-c), respectively. The model consists of a 65nm-thick gold (Au) V-antenna scatterer with a trace width of $w = 250$nm on a 10μm-thick silicon (Si) substrate embedded in 24μm-thick air domain. The setup mimics the "Scatterer on Substrate" COMSOL library model, utilizing the Wave Optics module and two Electromagnetic Waves, Frequency Domain (ewfd) physics environments. The first environment solves for the total field of the undecorated air/Si interface, $\boldsymbol{E}'_{tot}$, using periodic boundary conditions (PBCs) and periodic ports. The second adds in the scatterer and replaces the ports and PBCs with perfectly-matched layers (PMLs) to solve for the true scattered field $\boldsymbol{E}_{scat}$ using $\boldsymbol{E}'_{tot}$ from the first environment as the background field of the second, such that $\boldsymbol{E}_{scat} = \boldsymbol{E}_{tot} - \boldsymbol{E}'_{tot}$.

Note that this second environment does not include any periodicity, which is acceptable for this work. The assumption is that each scatterer will be placed far enough from nearest neighbors so that mutual coupling can be ignored. As a result, the unit cell periodicity was set to $a = 6\mu$m to be large enough to not interact with the PML, but small enough to limit the diffraction orders to ± 1.

The incident field was launched from the Si base into the $+\hat{z}$ direction towards the listening port at the top of the air domain. As shown in Figure 3, the central axis of the V-antenna was aligned to 45° in the *x*-*y* plane and the field was aligned in $+\hat{y}$ direction to equally excite the two fundamental modes of the V-antenna: a high-frequency symmetric mode which oscillates along the half-length of the dipole, and a lower-frequency antisymmetric mode which oscillates the length of the dipole. This way, when the antenna undergoes a 90° rotation to induce a 180° phase shift [2], the field components remain equally applied and there is no need to re-calibrate the incident field strength.

Both near-field (NF) and far-field (FF) data was collected. The NF was sampled using a Domain Point Probe located directly above the scatterer at 20μm away, which was verified as being an appropriate distance to approximate a plane wave. The Far-Field Calculation was used on the internal air/PML boundaries surrounding the model. This process projects the NF out to a

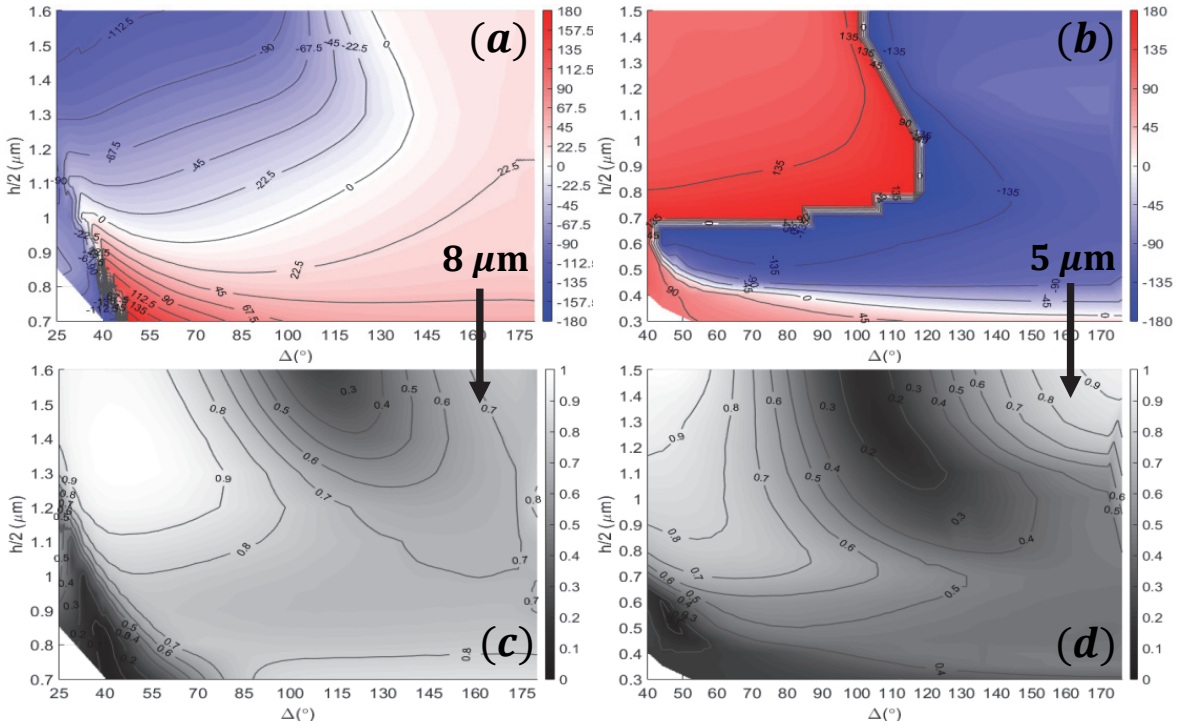

Figure 4. Interpolated COMSOL results for the parametric profiles and their nominal contours for phase $\boldsymbol{\phi}$ (a,b) and amplitude $\left|\boldsymbol{E}_{\boldsymbol{scat}}^{\boldsymbol{x-pol}}\right|$ (c,d) at designed operating wavelengths of 8μm (a,c) and 5μm (b,d).

distance where only the radiation fields (transverse to the radial direction of propagation) are important. The governing equation is termed the Stratton-Chu formulation, and COMSOL's form is given by:

$$\boldsymbol{E}_{FF}(\theta,\,\phi) = \frac{ik}{4\pi}\boldsymbol{r}_0 \times \int d\boldsymbol{S}\left[\boldsymbol{n}\times\boldsymbol{E} - \sqrt{\mu/\epsilon}\,r_0 \times (\boldsymbol{n}\times\boldsymbol{H})\right] e^{ik(\mathbf{r}\cdot\mathbf{r}_0)} \quad [4]$$

where $\boldsymbol{E},\boldsymbol{H}$ are the fields on the surface $\boldsymbol{S}$, (which is acting as the aperture), $\boldsymbol{r}_0$ is unit vector from origin to the observation point, $\boldsymbol{r}$ is the radius vector of $\boldsymbol{S}$, and $\boldsymbol{n}$ is a unit vector normal to $\boldsymbol{S}$. For COMSOL, $\boldsymbol{r}_0$ is set at 1m, which is important for understanding how it determines the FF phase.

Meshing was a primary concern in several regions of the model. Since the V-antenna was only 65nm thick, which is only about three skin depths into an Au layer for a field propagating in the M/LWIR, a Boundary Layer mesh of two layers was applied to the top and bottom of the element. Due to the nature of large field confinement in subwavelength plasmonic materials in this regime, an additional highly-compressed mesh was needed in a region about $\pm 1.5\mu$m around the interface to accurately resolve the scattered field, as shown in Figure 3(b). Finally, the PML mesh was assessed for variations in E_{scat}^{x-pol} due to the PML thickness and mesh density, indicating that a PML thickness greater than $a/3$ and mesh density less than $12/a$ resulted in unacceptable variance in the FF amplitude—though the NF remained relatively unchanged.

Solutions were calculated separately at 5μm and 8μm for preparation of lenses with different wavelength responses. The vertex angle (Δ) and half-dipole length ($h/2$) were scanned in steps of $\Delta = 4°$ and $\frac{h}{2} = 0.05\mu$m over the respective ranges of $25° - 180°$ and $0.7\mu\text{m} - 1.6\mu\text{m}$ for the 8μm solution and $40° - 180°$ and $0.3\mu\text{m} - 1.5\mu\text{m}$ for the 5μm solution. To effectively collect the data from this large parameter space, a Batch Sweep study was accomplished. Each solution was on the order of 40GB, with ~200K domain meshes and ~2.2M degrees of freedom. Using a 2 CPU/16-core/128GB workstation, this permitted three concurrent solutions running on 5 cores each, and each solution (encompassing both physics environments) took ~15 minutes.

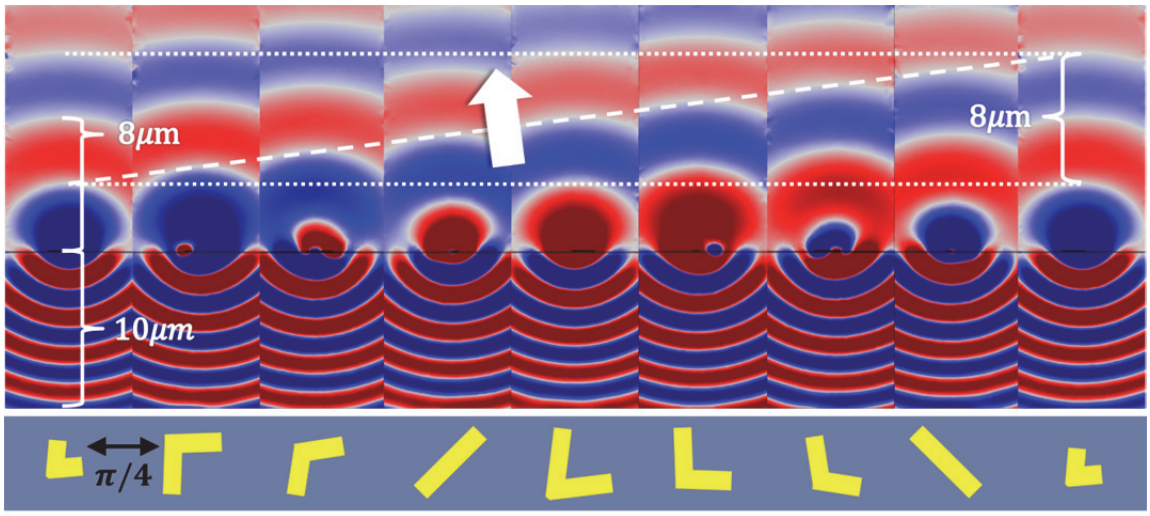

Figure 5. COMSOL demonstration of how a linear phase gradient along a metasurface made of 8 discrete elements phased $\boldsymbol{\pi/4}$ apart scatters an oblique plane wave (thick dashed) from a normally-incident pane wave.

4. COMSOL Simulation Results

The parametric profiles and their nominal contours are shown in Figure 4(a-d) for ϕ (a,b) and $\left|E_{scat}^{x-pol}\right|$ (c,d) at 8μm (a,c) and 5μm (b,d). These profiles were interpolated in MATLAB out to 500 data points, generated from the original COMSOL output, and the amplitudes were normalized to the maximum of the combined data set. A characteristic dipole resonance, where the scattered field amplitude drops, can be seen at regions of strong phase gradients. The steeper the phase shift, the larger the loss; this indicates areas to avoid in the selection process. As expected, the 5μm amplitude is lower on average than at 8μm due to the smaller scattering cross-section. This will lead to a less efficient lens unless the smaller characteristic length permits a larger packing density.

The scattered cross-polarized electric field from the COMSOL results can also be used to demonstrate the anomalous refraction generated from a linear phase gradient, as seen in Figure 5. Here, by selecting eight V-antenna geometries (bottom) as dictated by the profiles in Figure 4, a broadside plane wave can form from neighboring elements equally spaced one period apart and separated in phase by $\pi/4$. However, the elements are not all unique; elements 5-7 are a 90° CCW rotation of elements 2-4. This is due to the lack of phase and amplitude accessible by the given parameter space. The good news is, as referenced in Section 3, the symmetry in the V-antenna dictates that under 90° rotation it should produce an identical amplitude as the original with only a 180° phase shift. In this new configuration, the dipole arms are aligned with the field components such that the current flows the same distance along the same polarization vectors, but at differing times than the original, causing the phase difference.

From here, the COMSOL profiles were used as the input for algorithms used to produce the specific designs for the fabricated metasurfaces and lenses, which will be described in the next Section.

5. Lens Fabrication

While the importance of having an equally spaced phase shift is evident, it is also important to not just simply bin those elements that meet a given phase value and pick the one which possesses the maximum amplitude in that bin, as this maximum would be different for each chosen element, leading to variations in the scattered phase fronts due to incomplete constructive/destructive interference. Therefore, element selections for the fabricated devices were chosen based on an optimization algorithm, which finds for a given N the required relative phase difference $\Delta\varphi$ and maximum average

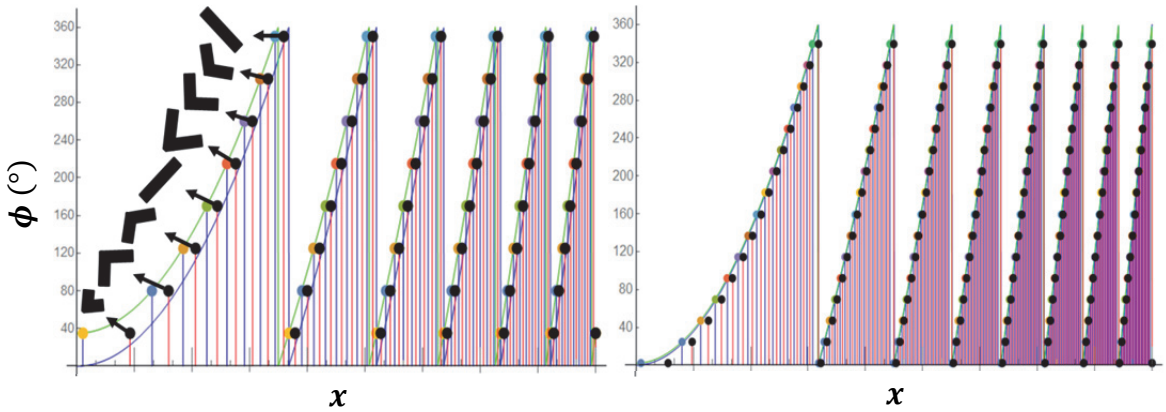

Figure 6. Phase (ϕ) calculation for example lens designs $\lambda_0 = 5\mu$m, $N = 8$, $f = 100$mm (left) and $\lambda_0 = 8\mu$m, $N = 16$, $f = 50$mm (right) used to identify the physical cut-offs of the phase regions. Black dots represent the midpoint values of Equation [3] which were used to better represent the deviation of the phase in a given region.

amplitude $\mathrm{Max}\big(\mathrm{Mean}(|E|)\big)$ to within desired tolerances, if it exists. If it does not exist, then the 90° rotated element of an existing corresponding element is used. Additionally, the code assessed the best starting phase value—representing the zero phase point—for all possible starting values from $\phi_0 = 0° \rightarrow 2\pi/N$. This algorithm provided a series of elements which had an amplitude deviation much smaller than previous published works [2, 4], while maintaining a deviation in relative phase shift of less than 1%.

The last piece of the puzzle was to determine the physical boundaries of the phase regions, which is given by solving for x_i in Equation [3], knowing all other parameters and setting $y = 0$, since this is a cylindrical lens. Examples of these phase calculations for two lenses of different focal lengths and different N are shown in Figure 6. The green line represents the direct phase calculation [3], while the blue line represents the normalization of this calculation to $\phi_0 = 0$, which is entirely valid, since the relative difference is what matters. The colored dots are the points $2\pi/i$, while the black dots have been shifted over in x to the midpoint position. The midpoints were selected as the region boundaries as they better represented the discretization of the constant phase regions[1].

The lens fabrication was accomplished at Sandia National Laboratories using a deep-UV photolithographic process. Nineteen unique lenses and eight unique metasurfaces were fabricated, varying several parameters, to include:

- Operating wavelength, $\lambda_0 (5/8\mu\mathrm{m})$
- $\mathcal{F}/\#$ $(5 - 40)$
- Number of unique elements, N $(8/16)$
- Packing density (intracell periodicity)

The investigation of a low $\mathcal{F}/\#$ is desired for "fast" lenses. The increase in N pushes the discretization to a much better approximation of the continuous phase gradient, and thus should provide improved focus. The higher packing density should improve the efficiency of coupling energy into the anomalous refractive mode.

SEM images in Figure 7 show (a) a full lens at diameter $d = 5$mm with design parameters

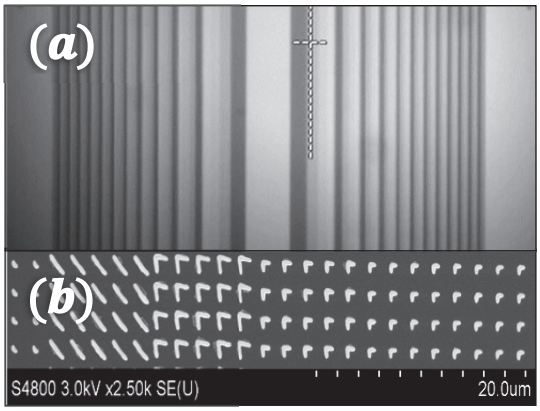

Figure 7. SEM image of a fabricated lens for 5μm, $N = 8$, $f = 100$mm (a) and a 250x close-up of a similar lens but with $N = 16$, showing the gradient of regions with constant phase (b).

[1] Analogous to the improvement gained from using the Midpoint Rule for a Riemann Sum.

$\lambda_0 = 5\mu$m, $N = 8$, $f = 100$mm and (b) a 250x magnified region for a lens of $\lambda_0 = 5\mu$m, $N = 16$, $f = 100$mm. The strong gradients generated by the variations in areal density can be seen clearly from the macroscopic view (a), and the logical progression of V-antenna geometries to induce a variation in phase can be seen in the microscopic view (b).

6. Discussion

The 8μm results are in good agreement with previous works [2, 11], with the major difference being a shift in the pattern to higher Δ and longer $h/2$ due to our 30μm thicker trace width. And while the 5μm results have no direct comparison in literature, both the phase and amplitude patterns are quite similar to the 8μm profile giving a high measure of confidence to the data. The glaring difference is where there is a crossover of the zero phase point in the 8μm profile, in the 5μm profile there is a crossover of the 180° phase point. This becomes an arbitrary viewpoint when one considers the effects of the 90° rotation, which in effect reverses this contrast (recorded, but not shown).

Measurements are currently in progress, which will illuminate the samples at λ_0 with a plane wave from a quantum cascade laser (QCL) while using a microbolometer array to scan along the optical axis and characterize the depth-of-field. This will spatially resolve the focal length and thus provide a validation of the COMSOL-based metasurface lens design process.

7. Conclusions

Through the use of COMSOL Multiphysics as a design/characterization tool, planar single-layer metasurface lenses were successfully recreated at 5μm and 8μm over the focal ratios $\mathcal{F}/5 - \mathcal{F}/40$ using variants of the seminal metasurface design. In the end, while an analytic approach is a more rapid solution for assessing simple geometries for metasurface lenses, COMSOL has demonstrated an equal ability to efficiently design these lenses, with the added benefit of an expanded functionality to more complex structures and architectures which analytical methods cannot address. This makes COMSOL a key asset in our future work of optimizing the metasurface lens performance.

8. References

[1] N. Yu and F. Capasso, "Flat optics with designer metasurfaces," *Nat Mater*, **13**, 139 (2014)

[2] N. Yu *et al*., "Light propagation with phase discontinuities: generalized laws of reflection and refraction," *Science*, **334**, 333 (2011)

[3] N. Yu *et al*., "Flat optics: controlling wavefronts with optical antenna metasurfaces," *IEEE J Quantum Elect*, **19**(3), 2341 (2013)

[4] F. Aieta *et al*., "Aberration-free ultrathin flat lenses and axicons at telecom wavelengths based on plasmonic metasurfaces," *Nano Lett*, **12**(9), 4932 (2012)

[5] F. Aieta *et al*., "Aberrations of flat lenses and aplanatic metasurfaces," *Opt Express*, **21**(25), 31530 (2013)

[6] C. Pfeiffer and A. Grbic, "Metamaterial Huygens' surfaces: tailoring wave fronts with reflectionless sheets," *Phy Rev Lett*, **110**, 197401 (2013)

[7] S. Sun *et al*., "Gradient-index metasurfaces as a bridge linking propagating waves and surface waves," *Nat Mater*, **11**, 426 (2012)

[8] F. Aieta *et al*., "Reflection and refraction of light from metasurfaces with phase discontinuities," *J Nanophotonics*, **6**(1), 063532 (2012)

[9] W. Wan *et al*., "Control the dispersive properties of compound plasmonic lenses," *Optics Communications*, **291**, 390 (2013)

[10] A. Pors *et al*., "Broadband focusing flat mirrors based on plasmonic gradient metasurfaces," *Nano Letters*, **13**, 829 (2013)

[11] R. Blanchard *et al*., "Modeling nanoscale V-shaped antennas for the design of optical phased arrays," *Phys Rev B*, **85**, 155457 (2012)

[12] F. Aieta *et al*., "Out-of-plane reflection and refraction of light by anisotropic optical antenna metasurfaces with phase discontinuities," *Nano Lett*, **12**(3), 1702 (2012)

[13] S. Larouche and D. R. Smith, "Reconciliation of generalized refraction with diffraction theory," *Opt Lett*, **37**(12), 2391 (2012)

9. Acknowledgements

We would like to acknowledge support from the Air Force Office of Scientific Research.